RESEARCH ARTICLE

Evaluating diffusion dispersion across an extended range of b-values and frequencies: Exploiting gap-filled OGSE shapes, strong gradients, and spiral readouts

Eric Seth Michael ⓘ | **Franciszek Hennel** ⓘ | **Klaas Paul Pruessmann** ⓘ

Institute for Biomedical Engineering, ETH Zurich and University of Zurich, Zurich, Switzerland

Correspondence
Eric Seth Michael, Institute for Biomedical Engineering, ETH Zurich and University of Zurich, Gloriastrasse 35, 8092 Zurich, Switzerland.
Email: michael@biomed.ee.ethz.ch

Purpose: To address the long echo times and relatively weak diffusion sensitization that typically limit oscillating gradient spin-echo (OGSE) experiments, an OGSE implementation combining spiral readouts, gap-filled oscillating gradient shapes providing stronger diffusion encoding, and a high-performance gradient system is developed here and utilized to investigate the tradeoff between b-value and maximum OGSE frequency in measurements of diffusion dispersion (i.e., the frequency dependence of diffusivity) in the in vivo human brain. In addition, to assess the effects of the marginal flow sensitivity introduced by these OGSE waveforms, flow-compensated variants are devised for experimental comparison.

Methods: Using DTI sequences, OGSE acquisitions were performed on three volunteers at b-values of 300, 500, and 1000 s/mm^2 and frequencies up to 125, 100, and 75 Hz, respectively; scans were performed for gap-filled oscillating gradient shapes with and without flow sensitivity. Pulsed gradient spin-echo DTI acquisitions were also performed at each b-value. Upon reconstruction, mean diffusivity (MD) maps and maps of the diffusion dispersion rate were computed.

Results: The power law diffusion dispersion model was found to fit best to MD measurements acquired at $b = 1000$ s/mm^2 despite the associated reduction of the spectral range; this observation was consistent with Monte Carlo simulations. Furthermore, diffusion dispersion rates without flow sensitivity were slightly higher than flow-sensitive measurements.

Conclusion: The presented OGSE implementation provided an improved depiction of diffusion dispersion and demonstrated the advantages of measuring dispersion at higher b-values rather than higher frequencies within the regimes employed in this study.

KEYWORDS
diffusion dispersion, diffusion MRI, high-performance gradient system, OGSE, restricted diffusion, spiral readout

1 | INTRODUCTION

The diffusion of water molecules is commonly exploited in MRI for the characterization of microstructural systems within which this motion occurs. In particular, there has been recent interest in detecting diffusion restrictions in such systems. A manifestation of this phenomenon can be observed in the spectral representation of diffusivity: as frequency ω increases (or, equivalently, as diffusion time decreases), spins encounter fewer and fewer microstructural entities, rendering diffusion less obstructed and apparent diffusivity higher. In order to detect this dispersion of diffusion,[1] the oscillating gradient spin-echo (OGSE) sequence[2,3] is often used. In contrast to a more typical pulsed gradient spin-echo (PGSE) experiment,[4] which employs a pair of monopolar, trapezoidal gradient pulses and sensitizes MR signal to diffusion at zero frequency, an OGSE measurement utilizes an oscillating diffusion-encoding gradient waveform and sensitizes the signal to diffusion at the frequency of the oscillations. Therefore, by piecing together a series of OGSE acquisitions, each with a unique frequency, the dependence of diffusivity on frequency can be observed, and the effects of diffusion restrictions relating to spectral properties can be quantified.

The translation of OGSE to in vivo human imaging occurred relatively recently due to practical considerations; gradient systems have only recently become strong enough to achieve both adequate diffusion sensitivity (i.e., moderate b-values) and high frequencies. In the first studies of the diffusion spectrum in the human brain, it was observed that diffusivity increased with frequency in gray and white matter regions.[5,6] Recent works have aimed to quantify this relationship more concretely in accordance with microstructural models: Arbabi et al[7] showed evidence of a $\omega^{0.5}$ dependence of the apparent diffusion coefficient consistent with either highly correlated structural disorder or short-range disorder along one dimension,[8] and Tan et al[9] found a linear dependence of diffusivity with respect to frequency in agreement with short-range disorder in two dimensions.[10]

This apparent discrepancy may be attributed in part to methodological factors (e.g., modeling choices), but the noise susceptibility endemic to OGSE measurements underlies such influences as a key confound; in relation to the clinical standard for diffusion imaging, OGSE severely lacks sensitivity. Clinical diffusion-weighted (DW) scans of the brain typically use b-values of 1000 s/mm², which optimizes sensitivity to variations among normal diffusivities in the brain, and can achieve such b-values in an echo time (TE) of about 50 ms for PGSE sequences using a modern clinical gradient system (80 mT/m amplitude). On the contrary, OGSE works focusing on the measurement of ω-dependent diffusivity in the in vivo human brain have only reached b-values up to 450 s/mm² with TEs in the range of 110-125 ms. Evidently, OGSE implementations will require upgrades in various domains to yield more reliable diffusion dispersion measurements and become better suited for clinical studies from a sensitivity standpoint.

Toward higher b-values, OGSE can be helped by using a high-performance gradient system, which can achieve greater diffusion sensitivity (and/or higher frequencies) for otherwise equivalent acquisition parameters. The aforementioned Tan et al study utilized such a gradient,[11] achieving $b = 450$ s/mm² for frequencies up to 100 Hz. Using a specialized gradient with similar specifications[12] for human brain OGSE imaging, we reached a b-value of nearly 1000 s/mm² in a similar echo time but at a lower maximum frequency (75 Hz),[13] albeit a frequency that has still not been reached with a standard gradient system. These examples represent the upper limits of frequency and b-value that have been achieved in published OGSE human brain experiments to date and highlight that there is an implicit tradeoff between these two parameters for a given TE: the highest oscillation frequency within a series of spectral measurements limits the b-value. It is worth noting that this compromise has yet to be explored experimentally in terms of sensitivity to the underlying frequency dependence.

Hardware aside, OGSE would benefit from improvements to acquisition and general sequence design in order to mitigate inherent weaknesses.[14] In the direction of enhancements to diffusion encoding, we have proposed gap-filled OGSE shapes, which extend the innermost gradient lobes in order to increase the b-value and frequency specificity at no cost to the echo time.[13] This improvement, however, adds a marginal flow sensitivity, which has not been fully investigated. In the direction of readout efficiency, a diffusion-prepared 3D gradient spin-echo sequence for oscillating diffusion gradients has been proposed to reduce overall scan time and improve the SNR.[15] Another potential avenue for readout-based sensitivity improvements would be to use spiral trajectories; to date, EPI is the only single-shot readout trajectory that has been used with OGSE. Compared with EPI, spiral readouts can provide a considerable SNR advantage because spirals have shorter TEs and better readout efficiency, among other favorable effects.[16]

Overall, various prospects exist with which oscillating gradient diffusion acquisitions can be enhanced. To realize the associated benefits, improvements to OGSE methodology in the domains of hardware and sequence design are implemented in this work for DTI of the in vivo human brain, as presented in recent conference abstracts:[17,18] we combine a high-performance gradient insert, gap-filled oscillating gradient waveforms, and, for the first time, spiral readouts. Using this

implementation, the spectral behavior of mean diffusivity (MD) is studied for frequencies up to 125 Hz and b-values up to 1000 s/mm², using a TE of only 95 ms for all scans. In particular, the tradeoff between b-value and maximum OGSE frequency is investigated by comparing diffusion dispersion fitting across different combinations of b-value and maximum frequency. Additionally, to explore the effect of the flow sensitivity introduced by gap-filled shapes, flow-compensated variants of these shapes are developed, and results are compared between the two cases.

2 | THEORY

2.1 | Oscillating gradient waveforms and power spectra

The logarithmic signal attenuation induced by an arbitrary diffusion-sensitizing gradient sequence $g(t)$ can be expressed as[19]

$$\ln\left(\frac{S_0}{S}\right) = \frac{1}{2\pi}\int_{-\infty}^{\infty} D(\omega)\,|F(\omega)|^2\,d\omega, \quad (1)$$

where S and S_0 are signals with and without diffusion weighting, respectively, $D(\omega)$ is the diffusion coefficient as a function of frequency ω, and $F(\omega)$ is the Fourier transform of the q-space trajectory $q(t)$,

$$F(\omega) = \int_{-\infty}^{\infty} q(t)\,e^{i\omega t}\,dt. \quad (2)$$

The q-space trajectory is the zeroth moment of $g(t)$,

$$q(t) = \int_{0}^{t} \gamma g(t')\,dt', \quad (3)$$

where γ is the gyromagnetic ratio. In effect, $F(\omega)$ is like a sampling function that dictates how contributions of $D(\omega)$ are weighted into the attenuated signal.[20] Therefore, to spectrally localize the signal loss and infer $D(\omega)$ at the desired frequency ω_0 with high precision, the gradient moment power spectrum $|F(\omega)|^2$ should consist of a pair of narrow lobes at frequencies $\pm\omega_0$ and have minimal spectral power elsewhere. Moreover, the b-value, which is given by the integral of the power spectrum,

$$b = \frac{1}{2\pi}\int_{-\infty}^{\infty} |F(\omega)|^2\,d\omega, \quad (4)$$

should be maximized relative to the gradient amplitude because the diffusion-encoding strength achieved in OGSE

experiments is typically suboptimal, especially for the gradient strengths of a clinical scanner.

To attain these specifications, trapezoidal[21] cosine-modulated OGSE shapes with apodized external lobes[3] and a timing correction[6] are often used, for which the power spectra consist of lobes at $\pm\omega_0$ with no zero-frequency contribution and minimal harmonics elsewhere. The modification to this sequence that we recently proposed[13] furthers this specificity by filling the oft-used half-period gap between pulses with elongated internal gradient lobes, thereby increasing both the b-value and the relative power in the $\pm\omega_0$ lobes; however, this alteration introduces a small contribution at zero frequency.

The introduction of a zero-frequency component entails that gap-filled OGSE waveforms have a non-zero first moment and, therefore, lack flow compensation; on the contrary, OGSE shapes without the modification are insensitive to flow. Importantly, flow-sensitive gradient sequences induce spin dephasing for microcirculatory flows in the ballistic regime (i.e., the second model of capillary networks in Le Bihan et al),[22] but this contamination reduces as the b-value increases and should be rather small in the brain due to the low perfusion fractions[23] and the small first moments of gap-filled OGSE waveforms.

To eliminate the residual flow sensitivity, a further modification to gap-filled OGSE shapes is developed here in the form of a timing correction: the penultimate lobe of the first gradient pulse is extended by a duration Δ_{FC}, and the final lobe of the first pulse is shortened by the same amount, thereby maintaining the pulse duration. The value of Δ_{FC} can be positive or negative (i.e., extending or shortening the penultimate lobe, respectively) and is defined by the condition that the integral of $q(t)$ reaches zero at the center of the refocusing RF pulse; a formula for Δ_{FC} in terms of other OGSE parameters is given in the Appendix. A time-reversed version of this timing correction is applied to the second gradient pulse, thereby guaranteeing that the q-space trajectory has zero integral over the entire diffusion-weighting gradient sequence and, therefore, that the sequence is flow-compensated.

As a further adjustment to the original gap-filled OGSE shapes, the external lobes of the diffusion-sensitizing gradient waveforms are no longer extended because the penultimate lobe modification achieves the same objective in reducing the zero-frequency spectral contribution.

To illustrate the OGSE waveform modification developed here as well as preexisting OGSE shapes, Figure 1 depicts examples of two-period oscillating gradient waveforms, corresponding q-space waveforms and their cumulative integrals, and power spectra for three variants of OGSE shapes. The transition from a standard OGSE shape
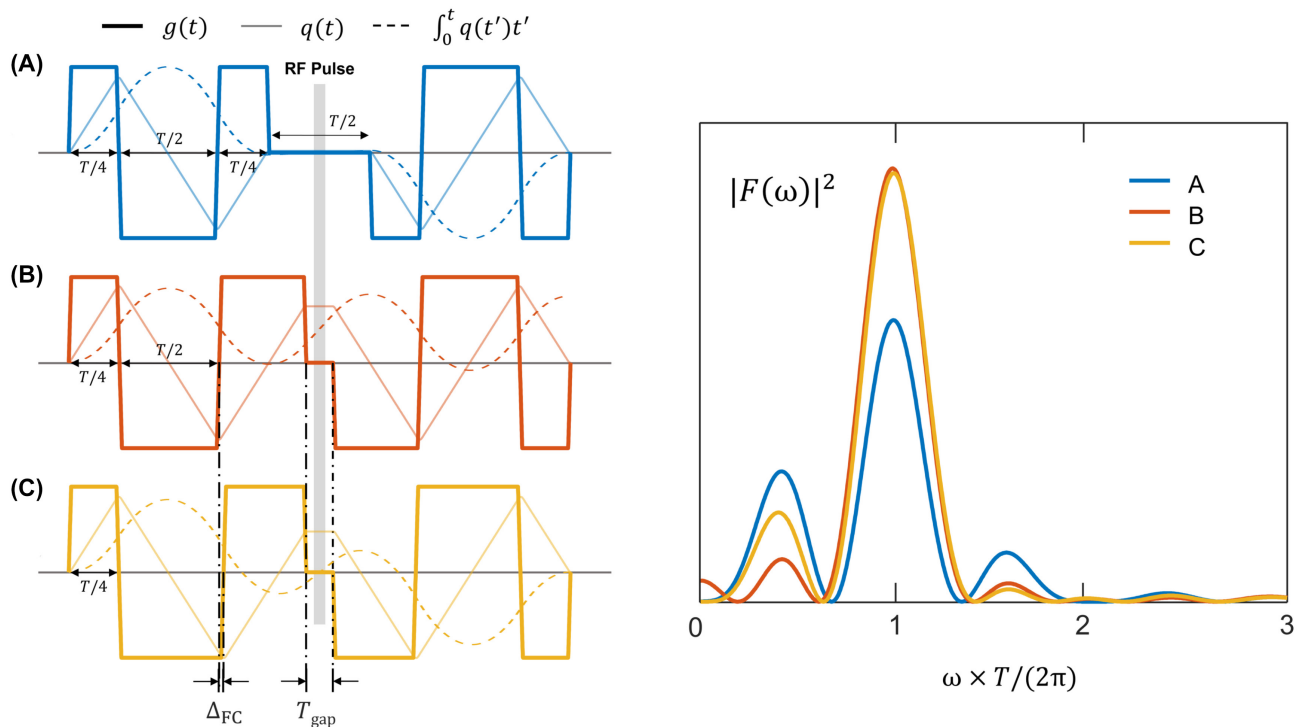
FIGURE 1 Comparison of OGSE gradient waveforms, their zeroth moments (q-space trajectories), and q-space cumulative integrals (left) and gradient moment power spectra (right). Each quantity is plotted for: (A) a standard OGSE waveform with a half-period gap and a correction to the external lobes to null the cumulative gradient area, (B) an original gap-filled OGSE shape with gap duration T_{gap}, and (C) a further modified gap-filled shape providing flow compensation. Like quantities are plotted to the same scale with units arbitrary. All OGSE gradient shapes have the same oscillation period T (corresponding to oscillation frequency $\omega_0 = 2\pi/T$) and amplitude. The second gradient pulse for each shape is a time-reversed and inverted version of the first gradient pulse, as gradient plots show effective shapes by accounting for the inversion of the first gradient pulse by the refocusing RF pulse. The outer lobes of gradient shapes (A) and (B) are specified as having durations of $T/4$ and $T/2$ for simplicity, but the timing corrections (which cannot be discerned on this scale) slightly alter their true durations. These shapes are plotted for 30 Hz waveforms with gradient amplitude 80 mT/m, slew rate 200 mT/m/ms, and gap duration 4.4 ms. Relative differences between the power spectra have only minor dependencies on these parameters and principally depend on the relative durations of a period, a ramp, and the gap

to the original gap-filled shape provides greater diffusion sensitization and a more specific measurement because the power spectrum of the latter has more energy and a more highly concentrated lobe at the target frequency; the enhanced spectral selectivity arises from the improved regularity of $q(t)$, particularly where the gap is filled. The ensuing flow-compensation timing correction to the original gap-filled shape results in a nulled zero-frequency component in the power spectrum owing to the zeroed integral of $q(t)$. At the expense of this improvement, however, the energy of the low-frequency lobe located between 0 and $\omega \times T/2\pi$ increases, which results in a slight increase in the b-value. Aside from these differences, the power spectra are practically identical for both gap-filled shapes. The relative spectral properties between gap-filled variants remain similar for waveforms with more oscillations, but the difference in low-frequency lobe energy between the two versions reduces as more periods are introduced. Additionally, Δ_{FC} becomes smaller then has its sign inverted as the number of oscillations increases.

2.2 | Advantages of spiral readouts

For general imaging considerations, spiral readouts inherently have shorter TEs than EPI readouts because of the center-out nature of the former. Furthermore, for spiral sequences combined with gap-filled OGSE shapes, the diffusion-encoding period exhibits temporal symmetry with respect to the 180° RF pulse, which is not the case for EPI sequences. This symmetry brings about two additional noteworthy advantages for spirals: the simplified construction of diffusion-sensitizing gradient waveforms that are immune to errors caused by concomitant gradient fields[24] and, of particular interest here, the possibility to eliminate the dead time before the onset of the diffusion gradients, thereby providing a further potential TE reduction relative to EPI scans. The total TE reduction of spiral acquisitions using gap-filled OGSE waveforms with respect to otherwise equivalent EPI acquisitions approximately equals the duration of the EPI readout; this feature is illustrated in Figure 2.
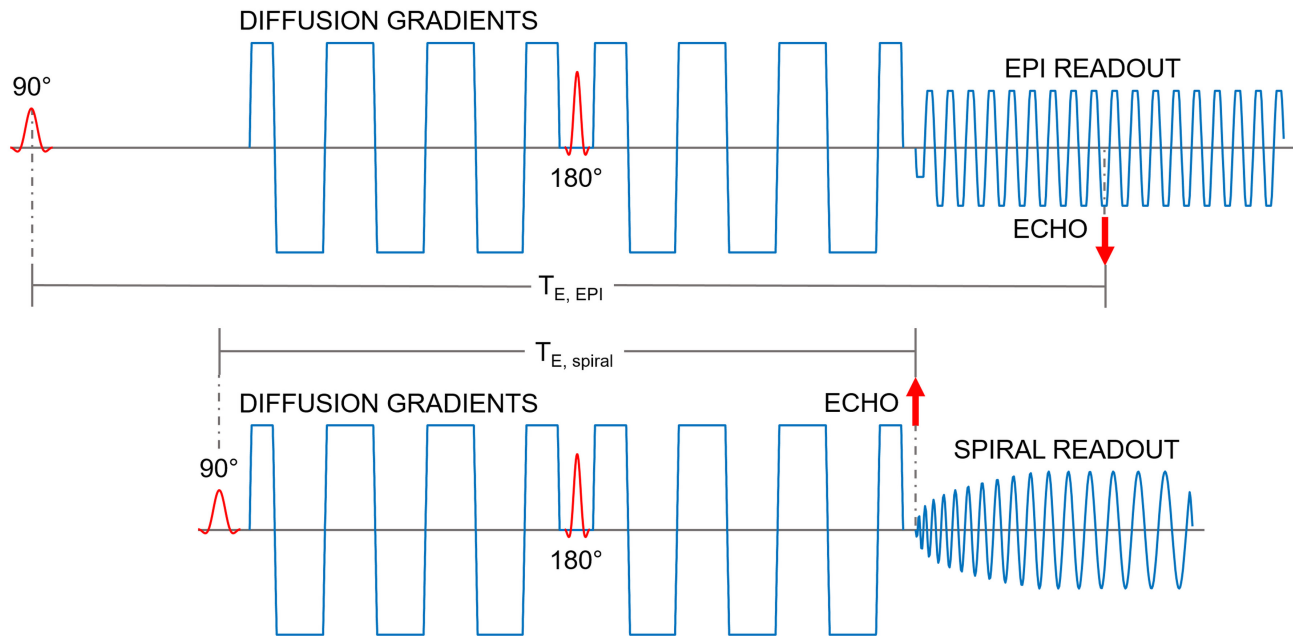
FIGURE 2 Sequence diagrams for gap-filled OGSE acquisitions with EPI (top) and spiral (bottom) readout. The timings of the diffusion gradients and the 180° RF pulse are identical for both readouts. Note that the 180° RF pulse cannot be repositioned within the diffusion-sensitizing gradient waveform

TABLE 1 Parameters for all OGSE waveforms used for phantom and human scanning

b-Value (s/mm^2)	Frequency (Hz)	Oscillation periods	Gradient amplitude (mT/m)	Flow compensation
300	30	1+1	46.2	Yes
			47.5	No
300	50	2+2	75.9	Yes
			76.8	No
300	75	3+3	118.5	Yes
			118.4	No
300	100	4+4	161.5	Yes
			160.2	No
300	125	5+5	199.8	Yes
			202.1	No
500	30	1+1	61.4	No
500	50	2+2	99.3	No
500	75	3+3	153.3	No
500	100	4+4	207.9	No
1000	30	1+1	84.5	Yes
			86.9	No
1000	50	2+2	139.4	Yes
			140.7	No
1000	75	3+3	218.6	Yes
			218.0	No

Note that gradient amplitudes slightly vary between flow-sensitive and flow-insensitive OGSE shapes of the same b-value and frequency. The gap duration was 4.36 ms for all scans except for the 125 Hz scans, for which the gap duration was 4 ms.

3 | METHODS

3.1 | Human brain and phantom scanning

Three healthy adult males volunteered for scanning in accordance with applicable ethics policy. A 5-L bottle-shaped water phantom doped with NaCl and $CuSO_4$ was also scanned for sequence calibration. Scanning was performed with a Philips 3T Achieva system (Philips Healthcare, Best, the Netherlands) equipped with a high-performance insert gradient coil that can reach gradient amplitudes up to 200 mT/m and slew rates up to 600 mT/m/ms at 100% duty cycle and an eight-channel RF transmit-receive array coil specifically designed for brain imaging with the gradient system.[25] The sequences used here, however, required a lower duty cycle, so the amplitude limit could be exceeded by up to 10%.

To evaluate the tradeoff between b-value and maximum frequency in diffusion dispersion measurements, an acquisition block was devised consisting of a series of OGSE DTI spiral sequences at different b-values and over different frequency ranges: acquisitions were performed at b-values of 300, 500, and 1000 s/mm^2 with all frequencies from a predetermined set (30, 50, 75, 100, and 125 Hz) up to 125, 100, and 75 Hz, respectively, using the original gap-filled waveforms with flow sensitivity. The gap duration, T_{gap}, was 4 ms for 125 Hz scans and 4.36 ms for scans at all other OGSE frequencies. The block also included PGSE DTI spiral sequences (representing 0 Hz, with an effective diffusion time of 39.1 ms) at all three b-values and was performed twice for each volunteer over separate scanning sessions to evaluate test–retest repeatability.

To assess the effects of flow compensation, additional $b = 300$ and 1000 s/mm^2 OGSE DTI spiral acquisitions with the flow-insensitive gap-filled waveforms devised here were performed during the initial scanning sessions of two of the volunteers using the same sets of frequencies and gap durations.

Finally, to compare the two readout trajectories, the flow-compensated OGSE DTI acquisition at $b = 1000$ s/mm^2 and 50 Hz was repeated using EPI readouts with the shortest possible TE for two of the volunteers in an additional scanning session.

For the three experiments described above, the total scan time per subject was 33 minutes (each session), 26 minutes, and 5 minutes, respectively. Table 1 provides parametric information about all OGSE waveforms used in these experiments. Additionally, it is worth noting that the first moment of each PGSE sequence was more than 5× larger than the greatest first moment among flow-sensitive OGSE sequences at the same b-value.

Each DTI protocol employed a multislice acquisition scheme and acquired 16 diffusion directions (the same direction scheme was used for each scan) and five $b = 0$ images. Other acquisition parameters were the same across all scans: 10 slices, 2 mm nominal in-plane resolution, 3 mm slice thickness, 2 mm interslice gap, TR = 5600 ms, TE = 95 ms (spiral) or 128 ms (EPI), and 2:03 minutes scan time. For all sequences, peripheral nerve stimulation (PNS) was reported to be minimal by all volunteers.

3.2 | Field monitoring and image reconstruction

Following scanning of both subjects and the phantom, a field camera based on ^{1}H NMR probes[26] (Skope Magnetic Resonance Technologies, Zurich, Switzerland) was placed in the scanner, and all sequences were repeated in order to monitor the spatiotemporal magnetic field evolution during each application of imaging gradients. Third-order spherical harmonic models were fitted to these data for each such instance and were used in conjunction with off-resonance maps in a higher-order algebraic reconstruction algorithm.[27] Reconstructed images were smoothed with a Hamming filter to mitigate Gibbs ringing and co-registered to correct for in-plane rigid body motion.

3.3 | b-Value correction

For each DTI image set, complete diffusion tensors were computed voxel-wise using the ordinary linear least-squares approach,[28] and maps of MD (i.e., the average of the three tensor eigenvalues)[29] were produced. The phantom MD data were then used to assess the fidelity of different diffusion-sensitizing gradient sequences. Differences between intended and actual b-values can occur due to gradient waveform inaccuracies, like those observed via field monitoring for imaging gradient sequences with the gradient system used here,[30,31] and manifest in differences between the measured and ground-truth diffusivity. Accordingly, the average MD in the phantom was computed for each OGSE and PGSE sequence (denoted MD_{seq}) and compared with the ground-truth frequency-independent phantom MD (denoted MD_{GT}), which was taken as the average MD among the three PGSE datasets at the center of the gradient coil. The apparent differences indicated deviations between actual and intended b-values. Consequently, in vivo diffusion tensors were isotropically scaled by the ratio MD_{GT}/MD_{seq} to provide a unique correction for each diffusion-sensitizing gradient shape.

3.4 | Data analysis

3.4.1 | Comparison of EPI and spiral results

For the matched EPI and spiral acquisitions, pure DW images for each DTI direction were computed, as well as the average DW image over all directions. To compare the noise susceptibility of OGSE acquisitions between the two readout trajectories, maps of the root-mean-square deviation (RMSD) of apparent diffusivity across DTI directions were computed. The RMSD calculation is given by

$$
\text{RMSD} = \sqrt{\frac{\sum_{n=1}^{N} \left(\frac{1}{b}\ln\left(\frac{S_0}{S_n}\right) - \text{Tr}\left(\mathbf{B}_n\mathbf{D}\right) \right)^2}{N - 6}}, \quad (5)
$$

where b is the b-value, S_n is the attenuated signal for the nth DTI direction, which has an associated normalized b-tensor $\mathbf{B}_n$, N is the number of DTI directions, and $\mathbf{D}$ is the (uncorrected) least-squares fitted diffusion tensor. It should be noted that 6 is subtracted in the denominator because a diffusion tensor has 6 degrees of freedom.

3.4.2 | Diffusion dispersion quantification

Using the flow-sensitive OGSE data, the spectral behavior of MD was modeled by the diffusion dispersion power law relationship based on recent results.[7] The power law model was fitted voxel-wise using the equation

$$
\text{MD}(\omega) = \Lambda\omega^\theta + \text{MD}_{\omega=0}, \quad (6)
$$

where Λ is the diffusion dispersion rate, $\text{MD}(\omega)$ is MD at frequency ω, $\text{MD}_{\omega=0}$ is the PGSE (0 Hz) MD, and structural disorder parameter $\theta = 0.5$ is assumed. In the model, Λ and $\text{MD}_{\omega=0}$ were the only free variables and were fitted to MD values from spiral acquisitions across all frequencies (including 0 Hz, per the convention of the model used to determine $\theta = 0.5$) as the least-squares solution. So-called diffusion dispersion maps depicting Λ were created based on the results of these fits. Separate fits/maps were computed for each b-value in order to compare results for different combinations of b-value and maximum frequency.

The diffusion dispersion model was also fitted to average MD values of manually segmented white matter tracts (guided by the ICBM-DTI-81 atlas),[32] once again separately for each b-value. The tract-wise results were used to assess test–retest repeatability by computing the differences in MD at each frequency and Λ between repetitions of the same subject for each b-value and tract. Squared differences were averaged across all subjects and tracts, and across all frequencies for MD, to provide cumulative measures for each metric and b-value, given as the normalized root-mean-square deviation (NRMSD).

3.4.3 | Effects of flow compensation

The diffusion dispersion mapping procedure was repeated for the flow-insensitive OGSE data, once again incorporating the PGSE measurements. The results were compared with the flow-sensitive data by performing paired t-tests using voxel-wise Λ for both cases as the paired samples; separate t-tests were performed for each subject and b-value. Equivalent t-tests were also performed to compare 75 Hz MD values. To omit CSF regions from the comparisons, the t-tests only included voxels for which MD $\leq 1.2 \times 10^{-3}$ mm^2/s across all measurements of the voxel used in the respective comparisons.

For reference, the systematic bias in measured MD caused by impurities in the spectral encoding profiles of flow-sensitive and flow-insensitive oscillating gradient shapes were compared between the two cases, as were the resulting biases in Λ estimated from multiple-frequency dispersion fits. These biases compare expected MD measurements that would result from the employed encoding profiles to MD values that reflect Dirac delta encodings, assuming that MD obeys pure $\omega^{0.5}$ dispersion.

3.5 | Diffusion dispersion error evaluation

As a complement to the in vivo diffusion dispersion fitting at different b-values, Monte Carlo simulations were performed to estimate the theoretical sensitivity of Λ measurements for the same b-value and frequency sets. MD measurements were simulated for each combination of the two parameters by sampling values from Gaussian distributions with means based on in vivo MD values and SDs computed using[33]

$$
\frac{D}{\sigma_D} = \text{SNR}_0\exp\left(-T_\text{E}/T_2\right)\frac{bD}{\sqrt{\frac{1}{N_{b=0}} + \frac{\exp(2bD)}{N_{b>0}}}}, \quad (7)
$$

where SNR_0 is the SNR of the $b = 0$ image, $N_{b=0}$ is the number of $b = 0$ acquisitions, and $N_{b>0}$ is the number of $b > 0$ acquisitions. For each b-value, all corresponding spectral measurements were simulated 100,000 times, where for each repetition the power law model in Eq. 6 was fitted to the simulated data. Subsequently, the mean and SD of the fitted dispersion rates could be computed for each b-value, from which respective dispersion-to-noise ratios (ΛNR) could be derived.

4 | RESULTS

4.1 | Comparison of spiral and EPI images

Figure 3 displays example images obtained from OGSE acquisitions at $b = 1000$ s/mm^2 and 50 Hz for both EPI and spiral readouts. The T_2- and diffusion-weighted image has higher intensity for the spiral sequence, and the individual and average diffusion-weighted images are smoother for the spiral acquisitions. Additionally, the MD map is less grainy for spiral readout, indicating a higher diffusion-to-noise ratio (DNR) for spiral than for EPI. The DNR advantage of the spiral acquisition can also be seen by its RMSD map, for which the average value is 26% lower than that of the EPI RMSD map, indicating less noise susceptibility in diffusivity measurements for spirals.

4.2 | Mean diffusivity against frequency and b-value

Figure 4 depicts MD maps for a representative imaging slice of one subject across all sampled b-values and frequencies for gap-filled OGSE waveforms without flow compensation; equivalent maps for the other two subjects are shown in Supporting Information Figure S1. Diffusivity of brain tissue increases as frequency increases

and as b-value decreases; CSF MD, on the other hand, decreases with both increasing frequency and b-value. Moreover, the DNR of these maps noticeably improves with stronger diffusion encoding, as the underlying regions are less speckled at higher b-values.

The observed trends can be seen more concretely in Figure 5, in which frequency-dependent MD values are plotted for example white matter regions of all volunteers and repetitions, and power law models are fitted for each b-value; plots showing these data averaged over volunteers and repetitions are shown in Supporting Information Figure S2. The MD values conform to the power law relationship at all b-values, with some minor exceptions likely resulting from parameter uncertainty and model imperfections. Across repetitions for each subject, the NRMSDs of the metrics were 7.1%, 5.1%, and 4.1% for MD and 38.0%, 17.4%, and 15.2% for Λ at $b = 300$, 500, and 1000 s/mm^2, respectively, indicating decreased variability with increasing frequency. Also, diffusivities are once again noticeably lower for higher b-values; the difference is exceptionally large going from $b = 500$ to 1000 s/mm^2. Plots of additional diffusion tensor metrics (e.g., fractional anisotropy) in these regions are provided in Supporting Information Figure S3.

Applying the power law model on a voxel-wise basis, Figure 6 shows diffusion dispersion maps of a representative imaging slice for each volunteer across all b-values for flow-sensitive OGSE data. In these maps, negative diffusion dispersion rates are masked, as this case is unphysical
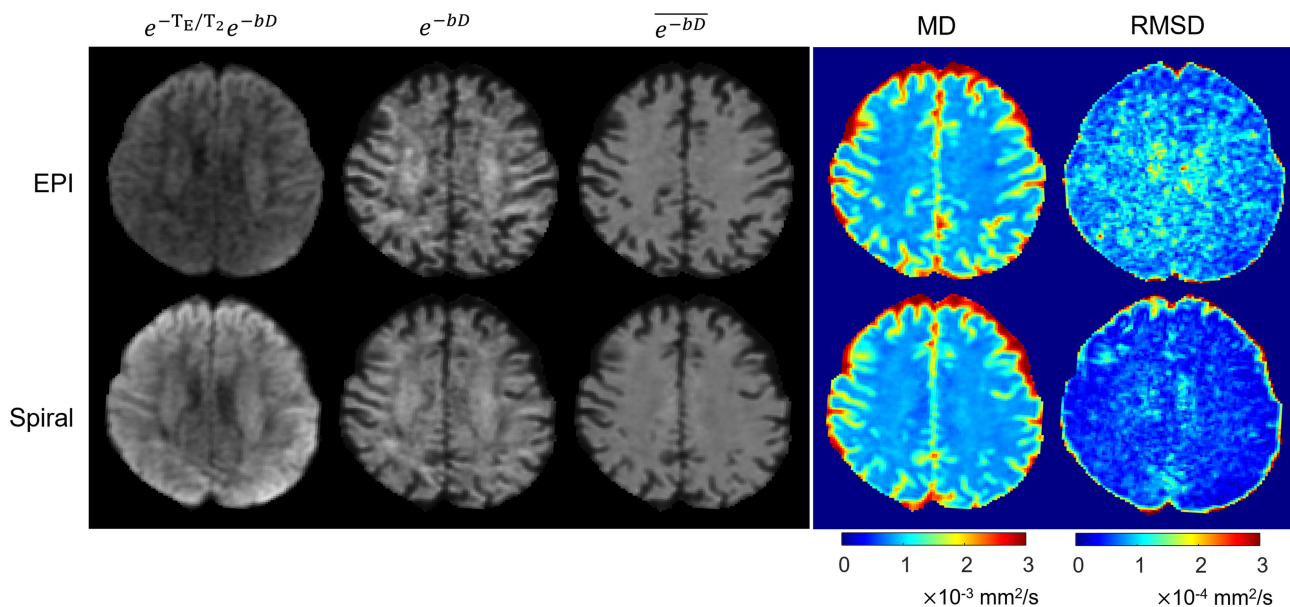

FIGURE 3 EPI (top row) and spiral (bottom row) images for flow-compensated OGSE DTI acquisitions at 50 Hz with $b = 1000$ s/mm^2. First column: T_2- and diffusion-weighted images. Second column: Diffusion-weighted images (i.e., T_2-weighting removed) for a single DTI direction. Third column: Mean diffusion-weighted images over all DTI directions. Fourth column: MD maps. Fifth column: Maps of the RMSD of apparent diffusivity measurements. Both rows of images depict approximately the same brain volume of one subject, but slight anatomical differences can be seen between rows because acquisitions of the different readout trajectories were acquired in separate scan sessions, leading to minor differences between the imaging volumes
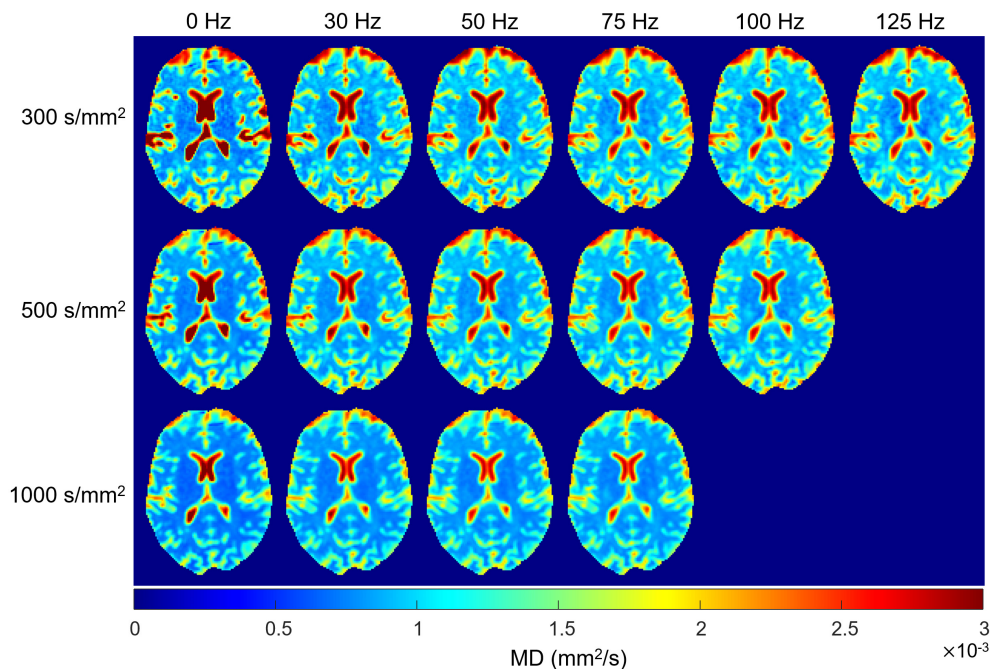
FIGURE 4 Representative MD maps across all b-values (different rows) and frequencies (different columns) for OGSE acquisitions without flow compensation

in tissue without flow where diffusion is hindered.[34] The masking condition used to omit CSF in the dispersion comparison is also applied. The parametric map quality greatly improves with increasing b-value; going from left to right, there is a strong tendency toward increasing local homogeneity in the diffusion dispersion rate. Additionally, the coverage of spurious regions, which are characterized by abnormally high diffusion dispersion rates or masked pixels, reduces with increasing b-value.

Figure 7 reports results of the Monte Carlo simulations, which yielded results consistent with the in vivo findings. Both ΛNR and ΛNR efficiency rise with increasing b-value, and the latter increments by greater margins due to the improved time-efficiency of sampling fewer frequencies.

4.3 | Impact of flow sensitivity on OGSE measurements

Figure 8 depicts example MD (75 Hz) and diffusion dispersion maps for both flow-sensitivity cases at $b = 300$ and 1000 s/mm^2. In the MD maps, areas with CSF have slightly higher diffusivities in the flow-insensitive case. Apart from CSF regions, MD maps at both b-values are qualitatively similar between the flow-sensitive and flow-insensitive data, such that relative contrast between different brain areas appears nearly the same for both cases. Likewise, diffusion dispersion rates appear similar between both cases at both b-values, with relative contrast maintained, but some differences can be

seen, especially in regions adjacent to masked areas, in which dispersion is incongruously high in only one case. Similar observations were made across all slices of both volunteers.

The quantitative comparisons, on the other hand, indicated statistically significant differences between the two cases: MD and Λ values were greater for the flow-insensitive data in all t-tests (with $p < 0.001$) by $1.22 \pm 0.56 \times 10^{-5}$ mm^2/s and 0.37 ± 0.23 μm^2/s$^{0.5}$, respectively. By comparison, the systematic bias analysis yielded higher expected MD for the flow-sensitive shapes at most frequencies and higher flow-sensitive Λ, and the same tendencies for $b = 300$ and 1000 s/mm^2; however, the theoretical errors were very small ($\leq 0.4\%$ for MD and $\leq 0.75\%$ for Λ, with respect to a ground truth representing MD$_{\omega=0}$ and Λ values measured in vivo) and correspond to differences between flow-sensitive and flow-insensitive metrics about an order of magnitude smaller than those observed in the brain. Therefore, systematic biases induced by spectral impurities do not explain the observed differences.

5 | DISCUSSION

The OGSE implementation presented here deployed spiral readouts for the first time in oscillating gradient diffusion imaging and used an improved diffusion sensitization scheme, forming an altogether time-efficient realization of the technique. The application of this methodology with
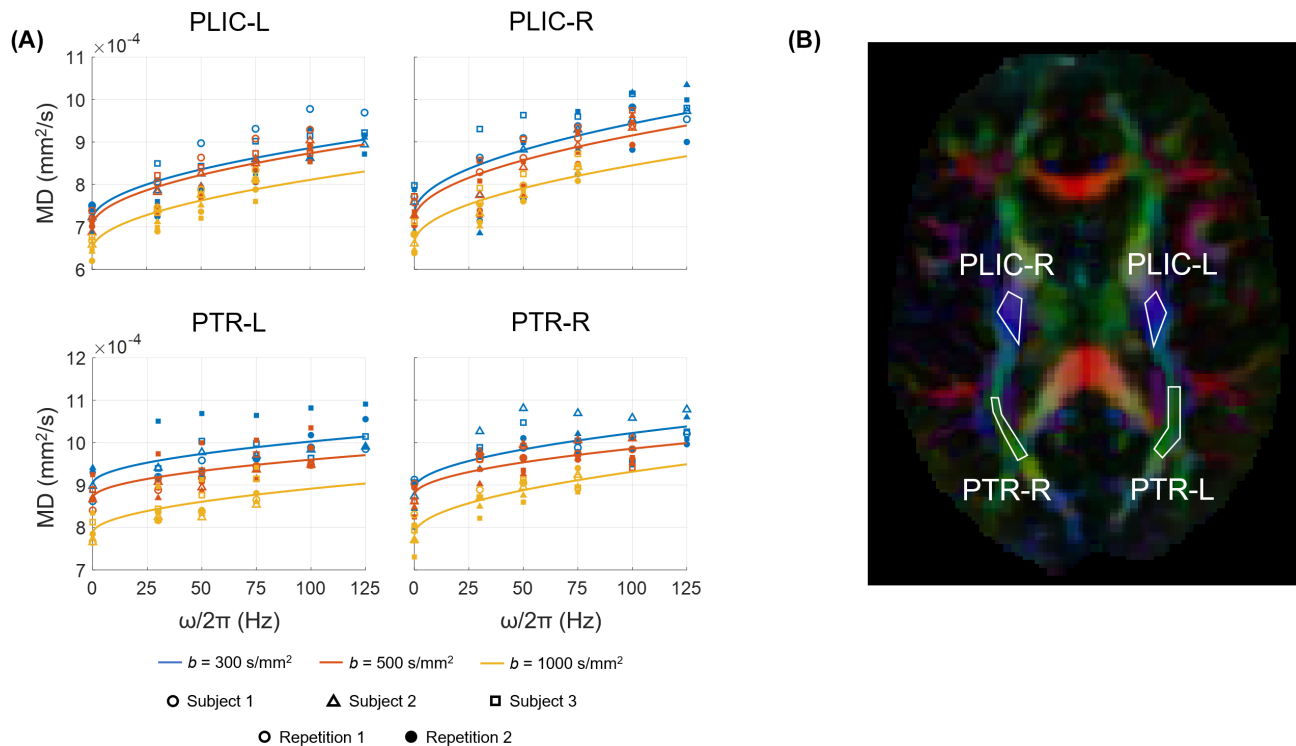
FIGURE 5 (A) Diffusion dispersion models (solid lines) fitted to region-wise average MD data (points) in example white matter regions. (B) Delineated white matter areas for an example colored fractional anisotropy map of one volunteer. In (A), the region-wise averages are plotted for both repetitions of all volunteers and b-values, and one curve is fitted per b-value for each region based on the average over all repetitions and volunteers. MD data at non-zero frequencies come from OGSE acquisitions without flow compensation. PLIC, posterior limb of the internal capsule; PTR, posterior thalamic radiation; L/R, left/right
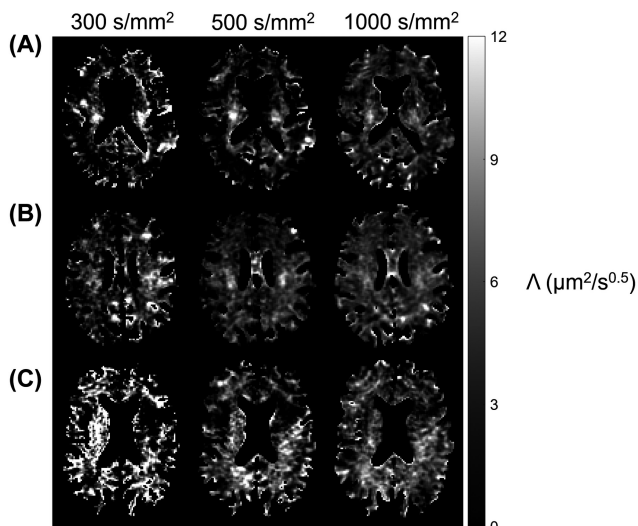

FIGURE 6 Diffusion dispersion maps for all b-values (different columns) for flow-sensitive OGSE acquisitions. A representative slice of each volunteer is shown (rows A, B, and C)

strong gradients permitted an assessment of diffusion dispersion in a regime of previously unreached frequencies and b-values.

In comparison to previous in vivo human brain OGSE studies, the data presented here correspond to comparable dispersion rates and are consistent with the relative steps in MD, namely, a larger step from 0 Hz to the first OGSE frequency than between OGSE frequencies.[5–7,9,13] Moreover, the data indicate a clear advantage of favoring higher b-values instead of a broader spectral range in measuring diffusion dispersion among the regime explored here (i.e., maximum frequency $\leq$ 125 Hz, $b \leq$ 1000 s/mm^2), which encompasses the parameter ranges used in all human OGSE studies to date. Evidently, the reduced noise sensitivity of the underlying MD maps outweighs the benefits of reaching higher frequencies: in particular, the increased maximum difference in diffusivity values and, based on what is typically done in practice, the increase in the number of intermediate frequencies that are sampled. This observed advantage is the first experimental demonstration involving the tradeoff between b-value and maximum frequency in OGSE measurements and suggests that further quantifications of diffusion dispersion (e.g., for different pathologies) will benefit by favoring b-value over maximum frequency to maximize sensitivity, an implication that is supported by the Monte Carlo error propagation analysis. This finding is also consistent with the linear error propagation analysis used by Arbabi et al, which indicated an advantage of compromising maximum frequency to increase b-value in a similar

frequency regime but for a more simplified consideration in which a single PGSE and a single OGSE scan are performed.[7] The scenario represented here, however, is likely
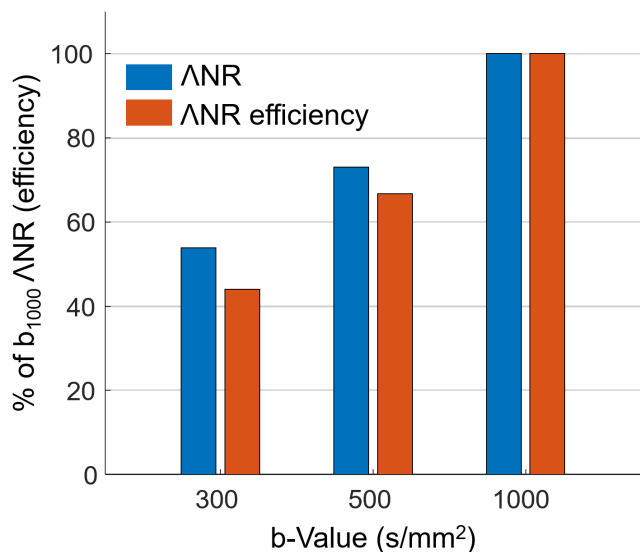

FIGURE 7 Relative ΛNR and ΛNR efficiency of multiple-frequency PGSE/OGSE acquisitions at different b-values. Parametric values assumed for the simulated MD measurements represent the data shown in Figure 5: $MD_{\omega=0} = 8.0 \times 10^{-4}$ mm²/s at $b = 1000$ s/mm² with increments of 0.5×10^{-4} mm²/s for the two reductions in b-value, $\Lambda = 6$ μm²/s$^{0.5}$ at all b-values, $SNR_0 = 65$, and $T_2 = 80$ ms. ΛNR, dispersion-to-noise ratio

more practical when the measurement of intermediate frequencies is necessary, such as when θ is not assumed.

The preference toward higher b-values is also supported by the associated reduction in degradation of the dispersion maps. As b-value increases, masked regions (which predominantly occur in or near CSF) reduce, and various areas adjacent to the masked regions exhibit fewer abnormalities: in particular, anomalously high dispersion rates that are not repeated across acquisitions. The abnormalities conceivably occur due to cardiac pulsation. Pulsatile motion can alter a voxel's CSF volume fraction across scans, thereby impacting its frequency-dependent MD because CSF has a notably higher diffusivity than brain tissue.[35] As such, dispersion rates in vulnerable regions may fluctuate across acquisitions due to these pulsation-induced CSF volume variations; however, dispersion maps are less susceptible to this effect as b-value increases because CSF regions become smaller and have lower MD, as in Figure 4.

b-Values much higher than 1000 s/mm² will likely reduce sensitivity to diffusion dispersion because the DNR of individual diffusivity measurements will deteriorate (based on Eq. 7), but such measurements are necessary to evaluate the dispersion of diffusion kurtosis.[36] Reaching frequencies beyond 125 Hz, on the other hand, will also result in DNR deficiencies, assuming that lower b-values would be used; however, because the best-fitting model for $D(\omega)$ depends on the sampled spectral regime,[37] higher frequencies may be
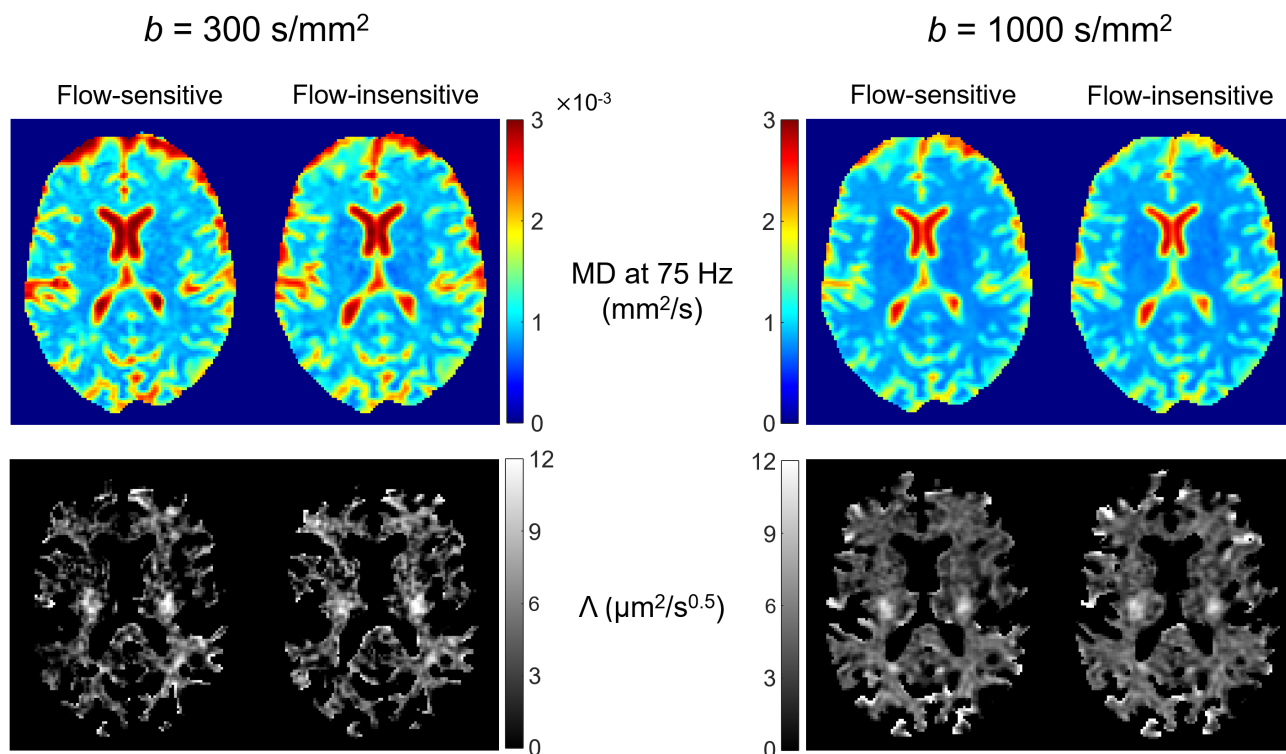

FIGURE 8 Maps of MD at 75 Hz (top row) and diffusion dispersion (bottom row) for a single slice of one subject for OGSE acquisitions with and without flow sensitivity at $b = 300$ and 1000 s/mm²

preferred to assess potential differences in behavior. That said, the new maximum frequency achieved in this work did not reveal anomalous behavior with respect to previous results, and the frequencies required to significantly expand this range, hardware permitting, will likely be limited by PNS.[9]

The OGSE measurements acquired using flow-compensated gap-filled shapes had higher MD (by 1-2%) and Λ (by 5-10%) with respect to the measurements using the flow-sensitive variants. This experimental result may seem unexpected because flow compensation eliminates the attenuation caused by ballistic flow and should thereby lead to lower MD and, thus, to lower apparent dispersion. However, the flow compensation may also lead to an opposing effect, which could result in greater MD and Λ for the flow-compensated measurements, because of the resulting increase of the sub-ω_0 sidelobe in $|F(\omega)|^2$ (see Figure 1). Importantly, this low-frequency spectral impurity may also contribute to perfusion-based signal attenuation because the effective $D(\omega)$ of microcirculation may contain sufficient power in this spectral range; the microcirculatory spectrum is expected to consist of a positive peak at zero frequency with a bandwidth up to tens of Hz.[38] As such, it may happen that the increase in attenuation caused by the larger low-frequency sidelobe in the flow-compensated $|F(\omega)|^2$ outweighs the reduction in attenuation caused by omitting the zero-frequency contribution, thereby leading to greater apparent diffusivity and, subsequently, higher dispersion for the flow-compensated measurements as a result of perfusion. That said, to ascertain whether perfusion is responsible for the observed MD and Λ differences would require further knowledge of the microcirculation spectrum, which has not yet been measured. It should also be noted that, even without perfusion, differences between diffusivities measured with flow-compensated and ordinary gap-filled OGSE pulses are expected due to differences between the spectral profiles of the pulses because $D(\omega)$ is not constant; however, as previously indicated, such expected differences are inconsistent with the observed differences in magnitude and direction when representative $\omega^{0.5}$ dispersion is assumed.

Eddy currents induced by strong oscillating gradient pulses can give rise to deviations between true and intended b-values and to signal losses through dephasing[39,40] in a way that depends on the extent of both forms of aberration and, therefore, on the specific diffusion-sensitizing gradient sequence. The phantom measurements indicated that such discrepancies occurred here, which were accounted for by correcting measured diffusion tensors via isotropic scaling; the phantom MD data are shown in Supporting Information Figure S4. Based on these data, the applied b-values were between -1.7% and $+3.3\%$ of the intended b-values and generally increased with increasing frequency and increasing b-value. The correction factors

did not account for potential temperature variations of the phantom during the experiment, but a subsequent analysis confirmed that diffusivity changes related to temperature variation occupied a range almost an order of magnitude narrower than those represented by the b-value corrections and could therefore be safely neglected.

A disadvantage of isotropic scaling is that b-tensor shape errors, such as those caused by gradient current miscalibration, are not accounted for. However, spatially averaged diffusion tensors of the phantom scans had fractional anisotropy values of 0.048 ± 0.014, which are an order of magnitude lower than the observed values in white matter and could therefore not greatly affect derived metrics. Moreover, although the spatial dependence of the applied b-value was neglected in this work, high-performance gradients are known to have stronger gradient nonlinearities and concomitant fields;[41] correcting for these spatial dependencies[42,43] would yield more accurate results.

An inter-slice gap was used here to cover a large portion of the brain while saving scan time, considering that the repetition rate of the diffusion gradients neared the gradient amplifiers' duty cycle limit. This approach is limited by sensitivity to through-plane motion, which may result in imperfect coincidence of the imaging volume across scans. For a gap-free acquisition in the same scan time, the maximum gradient amplitude would need to be reduced by about 10%, corresponding to a penalty in the b-value or maximum OGSE frequency.

6 | CONCLUSIONS

The OGSE implementation employed here, which utilized a high-performance gradient system with spiral readouts and improved oscillating diffusion-encoding gradient waveforms, permitted spectral diffusion measurements at higher b-values and frequencies and shorter TEs than can otherwise be achieved, thereby boosting diffusion sensitivity. Diffusion dispersion fits based on these measurements were found to particularly benefit from higher b-values. The improved reliability of diffusion dispersion measurements demonstrated here can facilitate further exploration of human brain microstructure and paves the way for broader implications of the spectral behavior of diffusion.

ORCID

Eric Seth Michael https://orcid.org/0000-0002-2513-4254
Franciszek Hennel https://orcid.org/0000-0003-0043-9921
Klaas Paul Pruessmann https://orcid.org/0000-0003-0009-8362

REFERENCES

1. Novikov DS, Kiselev VG. Effective medium theory of a diffusion-weighted signal. *NMR Biomed*. 2010;23:682-697.
2. Schachter M, Does MD, Anderson AW, Gore JC. Measurements of restricted diffusion using an oscillating gradient spin-echo sequence. *J Magn Reson*. 2000;147:232-237.
3. Does MD, Parsons EC, Gore JC. Oscillating gradient measurements of water diffusion in normal and globally ischemic rat brain. *Magn Reson Med*. 2003;49:206-215.
4. Stejskal EO, Tanner JE. Spin diffusion measurements: spin echoes in the presence of a time-dependent field gradient. *J Chem Phys*. 1965;42:288-292.
5. Van AT, Holdsworth SJ, Bammer R. In vivo investigation of restricted diffusion in the human brain with optimized oscillating diffusion gradient encoding. *Magn Reson Med*. 2014;71:83-94.
6. Baron CA, Beaulieu C. Oscillating gradient spin-echo (OGSE) diffusion tensor imaging of the human brain. *Magn Reson Med*. 2014;72:726-736.
7. Arbabi A, Kai J, Khan AR, Baron CA. Diffusion dispersion imaging: mapping oscillating gradient spin-echo frequency dependence in the human brain. *Magn Reson Med*. 2020;83:2197-2208.
8. Novikov DS, Jensen JH, Helpern JA, Fieremans E. Revealing mesoscopic structural universality with diffusion. *Proc Natl Acad Sci USA*. 2014;111:5088-5093.
9. Tan ET, Shih RY, Mitra J, et al. Oscillating diffusion-encoding with a high gradient-amplitude and high slew-rate head-only gradient for human brain imaging. *Magn Reson Med*. 2020;84:950-965.
10. Burcaw LM, Fieremans E, Novikov DS. Mesoscopic structure of neuronal tracts from time-dependent diffusion. *Neuroimage*. 2015;114:18-37.
11. Foo TKF, Tan ET, Vermilyea ME, et al. Highly efficient head-only magnetic field insert gradient coil for achieving simultaneous high gradient amplitude and slew rate at 3.0T (MAGNUS) for brain microstructure imaging. *Magn Reson Med*. 2020;83:2356-2369.
12. Weiger M, Overweg J, Rösler MB, et al. A high-performance gradient insert for rapid and short-T2 imaging at full duty cycle. *Magn Reson Med*. 2018;79:3256-3266.
13. Hennel F, Michael ES, Pruessmann KP. Improved gradient waveforms for oscillating gradient spin-echo (OGSE) diffusion tensor imaging. *NMR Biomed*. 2021;34:e4434.
14. Xu J. Probing neural tissues at small scales: recent progress of oscillating gradient spin echo (OGSE) neuroimaging in humans. *J Neurosci Methods*. 2021;349:109024.
15. Wu D, Liu D, Hsu Y-C, et al. Diffusion-prepared 3D gradient spin-echo sequence for improved oscillating gradient diffusion MRI. *Magn Reson Med*. 2021;85:78-88.
16. Lee Y, Wilm BJ, Brunner DO, et al. On the signal-to-noise ratio benefit of spiral acquisition in diffusion MRI. *Magn Reson Med*. 2021;85:1924-1937.
17. Michael ES, Hennel F, Pruessmann KP. Frequency and b-value dependence of the diffusion tensor in the human brain using enhanced oscillating gradient spin-echo (OGSE) sequences with 250 mT/m gradients. In Proceedings of the 37th Annual Meeting of ESMRMB, 2020. p. S122.
18. Michael ES, Hennel F, Pruessmann KP. Armance head gradient. In Proceeding time-efficient OGSE sequence with spiral readout for an improved depiction of diffusion dispersion. In Proceedings of the 2021 ISMRM & SMRT Annual Meeting, 2021. Abstract #0406.
19. Lundell H, Lasič S. Diffusion encoding with general gradient waveforms. In: Topgaard D, ed. *Advanced Difffusion Encoding Methods in MRI*. The Royal Society of Chemistry; 2020:12-67.
20. Gore JC, Xu J, Colvin DC, Yankeelov TE, Parsons EC, Does MD. Characterization of tissue structure at varying length scales using temporal diffusion spectroscopy. *NMR Biomed*. 2010;23:745-756.
21. Ianuş A, Siow B, Drobnjak I, Zhang H, Alexander DC. Gaussian phase distribution approximations for oscillating gradient spin echo diffusion MRI. *J Magn Reson*. 2013;227:25-34.
22. Le Bihan D, Breton E, Lallemand D, Aubin M-L, Vignaud J, Laval-Jeantet M. Separation of diffusion and perfusion in intravoxel incoherent motion MR imaging. *Radiology*. 1988;168:497-505.
23. Ahlgren A, Knutsson L, Wirestam R, et al. Quantification of microcirculatory parameters by joint analysis of flow-compensated and non-flow-compensated intravoxel incoherent motion (IVIM) data. *NMR Biomed*. 2016;29:640-649.
24. Baron CA, Lebel RM, Wilman AH, Beaulieu C. The effect of concomitant gradient fields on diffusion tensor imaging. *Magn Reson Med*. 2012;68:1190-1201.
25. Rösler MB, Leussler C, Brunner DO, et al. A transmit-receive array for brain imaging with a high-performance gradient insert. *Magn Reson Med*. 2020;84:2278-2289.
26. Dietrich BE, Brunner DO, Wilm BJ, et al. A field camera for MR sequence monitoring and system analysis. *Magn Reson Med*. 2016;75:1831-1840.
27. Wilm BJ, Barmet C, Pavan M, Pruessmann KP. Higher order reconstruction for MRI in the presence of spatiotemporal field perturbations. *Magn Reson Med*. 2011;65:1690-1701.
28. Basser PJ, Mattiello J, LeBihan D. MR diffusion tensor spectroscopy and imaging. *Biophys J*. 1994;66:259-267.
29. Basser PJ. Inferring microstructural features and the physiological state of tissues from diffusion-weighted images. *NMR Biomed*. 1995;8:333-344.
30. Hennel F, Wilm BJ, Roesler MB, Weiger M, Dietrich BE, Pruessmann KP. Echo-planar imaging of the human head with 100 mT/m gradients and high-order modeling of eddy current fields. *Magn Reson Med*. 2020;84:751-761.
31. Wilm BJ, Hennel F, Roesler MB, Weiger M, Pruessmann KP. Minimizing the echo time in diffusion imaging using spiral readouts and a head gradient system. *Magn Reson Med*. 2020;84:3117-3127.
32. Mori S, Oishi K, Jiang H, et al. Stereotaxic white matter atlas based on diffusion tensor imaging in an ICBM template. *Neuroimage*. 2008;40:570-582.

33. Xing D, Papadakis NG, Huang CL-H, Lee VM, Carpenter TA, Hall LD. Optimised diffusion-weighting for measurement of apparent diffusion coefficient (ADC) in human brain. *Magn Reson Imaging*. 1997;15:771-784.

34. Novikov DS, Fieremans E, Jespersen SN, Kiselev VG. Quantifying brain microstructure with diffusion MRI: theory and parameter estimation. *NMR Biomed*. 2019;32:e3998.

35. Baron CA, Beaulieu C. Acquisition strategy to reduce cerebrospinal fluid partial volume effects for improved DTI tractography. *Magn Reson Med*. 2015;73:1075-1084.

36. Yang GK, Tan ET, Fiveland E, Foo T, McNab J. Measuring time-dependent diffusion kurtosis using the MAGNUS high-performance head gradient. In Proceedings of the 2020 ISMRM & SMRT Virtual Conference, 2020. Abstract #0962.

37. Reynaud O. Time-dependent diffusion MRI in cancer: tissue modeling and applications. *Front Phys*. 2017;5:58.

38. Kennan RP, Gao J-H, Zhong J, Gore JC. A general model of microcirculatory blood flow effects in gradient sensitized MRI. *Med Phys*. 1994;21:539-545.

39. Ahn CB, Cho ZH. Analysis of eddy currents in nuclear magnetic resonance imaging. *Magn Reson Med*. 1991;17:149-163.

40. Barker BR, Archer BT, Erdman WA, Peshock RM. A MRI gradient waveform model for automated sequence calibration. *Med Phys*. 1992;19:1483-1489.

41. Jones DK, Alexander DC, Bowtell R, et al. Microstructural imaging of the human brain with a 'super-scanner': 10 key advantages of ultra-strong gradients for diffusion MRI. *Neuroimage*. 2018;182:8-38.

42. Lee Y, Kettinger AO, Wilm BJ, et al. A comprehensive approach for correcting voxel-wise b-value errors in diffusion MRI. *Magn Reson Med*. 2020;83:2173-2184.

43. Rudrapatna U, Parker GD, Roberts J, Jones DK. A comparative study of gradient nonlinearity correction strategies for processing diffusion data obtained with ultra-strong gradient MRI scanners. *Magn Reson Med*. 2021;85:1104-1113.

SUPPORTING INFORMATION

Additional supporting information may be found in the online version of the article at the publisher's website.

FIGURE S1 Representative MD maps for two volunteers (A and B) across all b-values (different rows) and frequencies (different columns) for OGSE acquisitions without flow compensation

FIGURE S2 Frequency-dependent MD (points) and respective diffusion dispersion models (solid lines) for white matter areas (shown in Figure 5B). Points are plotted for each b-value, representing the averages over volunteers and repetitions of region-wise means, based on the data shown in Figure 5, and one curve is fitted per b-value based on these points. MD data at non-zero frequencies come from OGSE acquisitions without flow compensation. PLIC, posterior limb of the internal capsule; PTR, posterior thalamic radiation; L/R, left/right

FIGURE S3 Additional frequency-dependent diffusion tensor metrics for white matter areas (shown in Figure 5B). Points are plotted for each volunteer and b-value, indicating the average over both repetitions of the region-wise mean. A line is drawn for each b-value, connecting the subject-wise average metric at each frequency. Data at non-zero frequencies come from OGSE acquisitions without flow compensation. AD, axial diffusivity; RD, radial diffusivity; FA, fractional anisotropy; PLIC, posterior limb of the internal capsule; PTR, posterior thalamic radiation; L/R, left/right

FIGURE S4 Frequency dependence of MD in the water phantom. Mean MD is plotted for each frequency and b-value (with and without flow compensation), taken as the average MD over the imaged volume of the phantom. Plotted values were used in the b-value corrections. FC, flow-compensated; NFC, not flow-compensated

---

How to cite this article: Michael ES, Hennel F, Pruessmann KP. Evaluating diffusion dispersion across an extended range of b-values and frequencies: Exploiting gap-filled OGSE shapes, strong gradients, and spiral readouts. *Magn Reson Med*. 2022;87:2710–2723. doi:10.1002/mrm.29161

APPENDIX

The duration (in seconds) by which the penultimate gradient lobe of the first pulse must be extended to achieve flow insensitivity is given by

$$\Delta_{\text{FC}} = \frac{T}{2} - \frac{1}{2}\sqrt{\frac{4sG^2 + 8aG + 7sT^2 + 8aT(2p+0.5)}{8s}} \text{ iff } 2p \text{ even,}$$

$$\Delta_{\text{FC}} = \frac{T}{2} - \frac{1}{2}\sqrt{\frac{4sG^2 + 8aG + 9sT^2 - 8aT(2p+0.5)}{8s}} \text{ iff } 2p \text{ odd,}$$

where p is the number of periods in each pulse (i.e., an integer or an integer and a half), T is the period of the oscillating waveform in seconds, s is the slew rate in T/m/s, G is the duration of the gap between gradient pulses in seconds, and a is the gradient amplitude in T/m.